ease, experimental autoimmune encephalomyelitis (*2*), in T cells in demyelinating plaques from brains of patients with multiple sclerosis (*3*), and on T cells along the body's surface like skin, the tongue, and vagina (*14*). A recent study indicates oligoclonality of TCR expression in bulk cultures of TILs analyzed by Southern (DNA) blots (*15*). Also some alloreactive and virus-specific cytotoxic T cells use restricted TCR genes (*16*). Our data indicate that TILs may have a restricted TCR repertoire. If the TILs expressing $V_\alpha 7$ are involved in an antitumor response, specific culture of such cells could be advantageous in tumor therapy. Moreover, the technology should be useful for analysis of TILs within other types of solid tumor.

REFERENCES AND NOTES

1. S. A. Rosenberg, P. Spiess, R. Lafreniere, *Science* **233**, 1318 (1986); P. J. Spiess, J. C. Yang, S. A. Rosenberg, *J. Natl. Cancer Inst.* **79**, 1067 (1987); A. Anichini, A. Mazzocchi, G. Fossati, G. Parmiami, *J. Immunol.* **142**, 3692 (1989); S. L. Topalian, D. Solomon, S. A. Rosenberg, *ibid.*, p. 3714; R. J. Barth, Jr., S. N. Bock, J. J. Mule, S. A. Rosenberg, *ibid.* **144**, 1531 (1990).
2. S. Zamvil *et al.*, *Nature* **317**, 355 (1985); H. Acha-Orbea *et al.*, *Cell* **54**, 263 (1988); J. L. Urban *et al.*, *ibid.*, p. 577.
3. J. R. Oksenberg *et al.*, *Nature* **345**, 344 (1990).
4. M. C. Miceli and O. J. Finn, *J. Immunol.* **142**, 81 (1989).
5. J. Y. Niederkorn, *Invest. Ophthalmol. Visual Sci.* **28**, 1397 (1987); R. Harning, G. C. Koo, J. Szalay, *ibid.* **30**, 1909 (1989); D. H. Char *et al.*, *N. Engl. J. Med.* **291**, 274 (1974).
6. F. H. Newton, *Arch. Ophthalmol.* **73**, 198 (1965); J. A. Shields, J. J. Augsburger, L. A. Donoso, V. B. Bernardino, M. Portenar, *Am. J. Ophthalmol.* **100**, 666 (1985); E. Fuchs, *Arch. Klin. Ophthalmol.* **77**, 304 (1910); O. A. Jensen, S. R. Anderson, *Acta Ophthalmol.* **52**, 173 (1974).
7. K. M. Egan, J. M. Seddon, R. J. Glynn, E. S. Gragoudas, D. M. Albert, *Surv. Ophthalmol.* **32**, 239 (1988).
8. The histological tumor types of the specimens were (by case number) (1) spindle B, (2) epithelioid, (3) mixed, (4) mixed, (5) mixed, (6) spindle B, (7) mixed, and (8) spindle B.
9. H-R. Rodewald, V. H. Koszinowski, K. Eichman, I. Melchers, *J. Immunol.* **143**, 4238 (1989); P. A. Morel, A. M. Livingstone, C. G. Fathman, *J. Exp. Med.* **166**, 583 (1987).
10. R. K. Saiki *et al.*, *Science* **230**, 1350 (1985); S. J. Scharf, G. T. Horn, H. A. Erlich, *ibid.* **233**, 1076 (1986); R. K. Saiki, T. L. Bungawan, G. T. Horn, K. B. Mullis, H. A. Erlich, *Nature* **324**, 163 (1986).
11. Total RNA from melanoma tissues was prepared in the presence of guanidium thiocyanate RNA Zol (Cima/Bioteox, Friendswood, TX) (*16*). Total RNA (2 μg) was used for the synthesis of single-strand cDNA with the use of reverse transcriptase. Briefly, in a final volume of 20 μl 1× PCR buffer [50 mM KCl, 20 mM tris-Cl (pH 8.4), 2.5 mM $MgCl_2$], 1 mM of deoxyribonucleotide triphosphates (Perkin-Elmer Cetus), 20 units of RNasin (Bethesda Research Laboratories), 100 pmol of random hexamer (Pharmacia), and 200 units of M-MuLV reverse transcriptase (Bethesda Research Laboratories) were incubated with RNA (2 μg) for 40 min at 42°C, as described in E. S. Kawasaki *et al.*[*Proc. Natl. Acad. Sci. U.S.A.* **85**, 5698 (1988)]. The reaction mixture was heated at 95°C for 5 min, then quickly chilled on ice. Thereafter each cDNA was used for PCR amplification.
12. T. M. Rose *et al.*, *Proc. Natl. Acad. Sci. U.S.A.* **83**, 1261 (1986).
13. Y. Yoshikai, N. Kimura, B. Toyonaga, T. W. Mak, *J. Exp. Med.* **114**, 90 (1986).
14. S. Itohara *et al.*, *Nature* **343**, 754 (1990).
15. A. Belldegrun, A. Kasid, M. Uppenkamp, S. L. Topalian, S. A. Rosenberg, *J. Immunol.* **142**, 4520 (1989).
16. A. Winoto *et al.*, *Nature* **324**, 679 (1986); V. Hochgeshwender, H. U. Weltzien, K. Erichmann, R. B. Wallace, J. T. Epplen, *ibid.* **322**, 376 (1986); R. Garman, J. L. Ko, C. D. Vulpe, D. H. Raulet, *Proc. Natl. Acad. Sci. U.S.A.* **83**, 3987 (1986); F. Rupp, H. Acha-Orbea, H. Henartner, R. Zinkernagel, R. Joho, *Nature* **315**, 425 (1986). M. Blackman *et al.*, *Cell* **47**, 349 (1986); Y. Choi *et al.*, *Proc. Natl. Acad. Sci. U.S.A.* **86**, 8941 (1989).
17. The oligonucleotide probe of $V_\alpha 7$ was labeled with the use of [γ-^{32}P]adenosine triphosphate (Du Pont Biotechnology Systems) and polynucleotide kinase. Unincorporated nucleotide was removed by means of a Sephadex G-25 column (Boehringer Mannheim).
18. J. Sambrook, E. F. Fritsch, T. Maniatis, *Molecular Cloning: A Laboratory Manual* (Cold Spring Harbor Laboratory, Cold Spring Harbor, NY, ed. 2, 1989).

19. We thank R. Bell, R. Mantegazza, K. Sakai, and L. R. Atalla for their helpful comments and assistance in carrying out this work. We thank R. Rappuoli, G. Peltz, A. Krensky, C. Clayberger, and T. de Magistris for allowing us to study V_α TCR expression in T cell clones. We appreciate T. Montgomery's assistance. This work was supported in part by the Phil N. Allen Trust. T.N. and J.R.O. are fellows of the National Multiple Sclerosis Society (U.S.A.).

20 March 1990; accepted 22 May 1990

Regional Variation of Extracellular Space in the Hippocampus

CHRIS J. MCBAIN, STEPHEN F. TRAYNELIS,* RAYMOND DINGLEDINE

The factors responsible for the unusual susceptibility of the hippocampus to seizures and ischemic cell damage are not well understood. The CA1 pyramidal subfield of the hippocampus is particularly vulnerable to seizure activity and damage after ischemia. The possibility was examined that regional differences exist in extracellular volume, which might influence neuronal excitability and response to injury in the hippocampus. CA1 stratum pyramidale exhibited an exceptionally low extracellular volume fraction (EVF) of 0.12, whereas the EVFs of CA3 and dentate were considerably higher—0.18 and 0.15, respectively. The EVF of CA1 stratum pyramidale was reversibly reduced by 30 percent when the extracellular potassium concentration was raised from 3.5 to 8.5 mM, a procedure that induced spontaneous electrographic seizures in CA1. Thus there are regional variations in the properties of the extracellular space in the hippocampus that might underlie the propensity of the CA1 region to develop seizures and to suffer damage after ischemia.

THE EXTRACELLULAR VOLUME FRACTION and tortuous diffusion pathways set fundamental constraints on the movement of ions and other substances within the interstices of the mammalian brain (*1*). Most estimates of EVF, made with a variety of techniques in several species and brain regions, fall within a narrow range of 0.17 to 0.22 (*1, 2*). Conditions that result in shrinkage or expansion of extracellular space have long been suspected of influencing neuronal activity (*3–5*). For example, shrinkage of extracellular space could, if large enough, enhance neuronal synchronization as a result of stronger electric field interactions and by a volume effect amplify the transient elevations in the extracellular potassium concentration ($[K^+]_o$) and transmitter concentrations that develop during neuronal activity (*4, 6–8*). The aim of this study was to make quantitative measurements of EVF and tortuosity (*9*) within the various layers of the hippocampal slice under both physiological and pathological conditions. We calculated the volume fraction and tortuosity of extracellular space in rat hippocampal slices (*10*) by the method of Nicholson and Phillips (*1*). Briefly, an ion-selective electrode was used to measure in real time the diffusion profile of an iontophoretically applied ion, tetramethylammonium (TMA^+), that is restricted to the extracellular compartment (Fig. 1A). The time-dependent rise and fall of the extracellular concentration of TMA^+ (Fig. 1B) is then fitted to a radial diffusion equation modified to account for EVF and tortuosity (*11*). The movement of TMA^+ within all regions of the hippocampus that we tested was well fit by the diffusion equation, irrespective of iontophoretic current intensity (Fig. 1B) or electrode spacing (*12*). Both EVF and tortuosity showed considerable regional variation (Table 1). The EVF of CA3 stratum pyramidale (0.18) was within the usual range (*1, 2*), but EVF of CA1 st. pyramidale (0.12) was 33% smaller (Fig. 1C

Department of Pharmacology, University of North Carolina at Chapel Hill, Chapel Hill, NC 27599.

*Present address: University College London, Gower Street, London WC1E 6BT.

and Table 1). The values of EVF in the other regions ranged between these values (*13, 14*). The tortuosity was also significantly different between CA1 and CA3. These results indicate that extracellular space in the CA1 region, especially in st. pyramidale, is very restricted.

Intraventricular injection of K^+ sufficient to raise $[K^+]_o$ to between 5.4 and 8.1 mM induces hippocampal seizures in cats (*15*). Similarly, hippocampal slices bathed in 8.5 mM $[K^+]_o$ undergo intense electrographic seizures that arise in and are restricted to the CA1 region. Such seizures are readily blocked by osmotic expansion of the extracellular space (*7*). Much larger increases in $[K^+]_o$, for example, those accompanying spreading depression (*5*) or seizures (*4*), are buffered by glial cells, which results in subsequent water movement into surrounding cells and thus a reduction of the EVF (*4*). It is unclear, however, whether a significant reduction in EVF would result from a rise in $[K^+]_o$ in the absence of intense neuronal firing. We tested this hypothesis directly by generating TMA^+ diffusion curves in hippocampal slices as $[K^+]_o$ was raised from 3.5 to 8.5 mM (Fig. 2). In high $[K^+]_o$, EVF was reduced in st. pyramidale of both CA1 (30.3 ± 5.0% decline) and CA3 (29.9 ± 5.4% decline) with no significant change in tortuosity (Fig. 2, A and B, and Table 2).

Table 1. Regional variation in extracellular space. Values are the mean ± SEM.

Region	EVF	Tortuosity	*n*
CA1 st. pyramidale	0.119 ± 0.018*	1.67 ± 0.03*	45
CA1 st. radiatum	0.132 ± 0.025*	1.71 ± 0.04*	30
CA3 st. pyramidale	0.177 ± 0.028	1.83 ± 0.04	41
CA3 st. radiatum	0.155 ± 0.028	1.71 ± 0.04*	31
st. granulosum	0.148 ± 0.030	1.80 ± 0.07	25

*The *F*-ratio obtained from ANOVA was significant, post hoc tests used a multiple comparison analysis against CA3 st. pyramidale and were considered significantly different at $P < 0.05$.

Table 2. Elevated K^+ restricts extracellular space in CA1 and CA3 st. pyramidale. Values are the mean ± SEM.

K^+ concentration	EVF	Tortuosity	*n*
	CA1 st. pyramidale		
3.5 mM	0.131 ± 0.035	1.65 ± 0.05	15
8.5 mM	0.088 ± 0.024*	1.69 ± 0.05	15
3.5 mM (recovery)	0.120 ± 0.033	1.81 ± 0.07	14
	CA3 st. pyramidale		
3.5 mM	0.187 ± 0.063	1.96 ± 0.09	10
8.5 mM	0.132 ± 0.044*	2.01 ± 0.10	10
3.5 mM (recovery)	0.200 ± 0.073	1.94 ± 0.09	9

*$P < 0.05$, *t* test compared with both control and recovery.

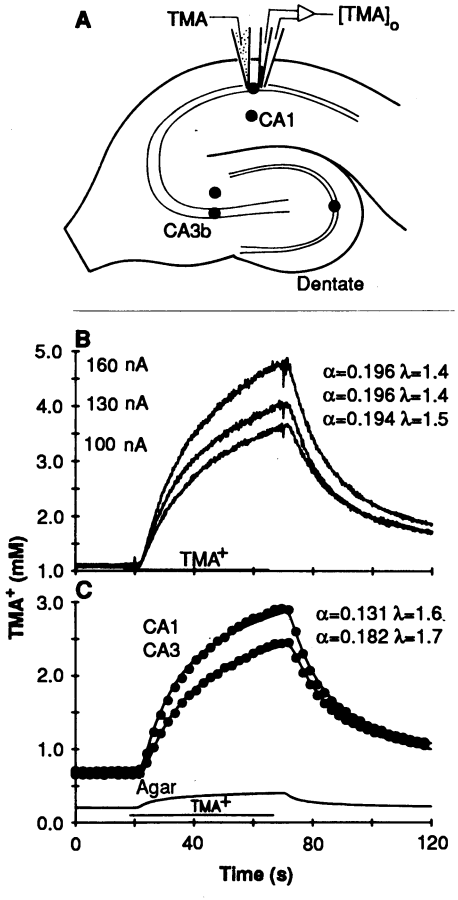

Fig. 1. Regional variation in EVF. (**A**) The electrode array and recording sites (solid dots) within the hippocampal slice. Iontophoretic and sensing electrodes were positioned parallel to the cell layer at a depth of 150 μm. The five dots show the recording positions in each subregion. Baseline extracellular TMA^+ concentration rose during the +20-nA steady bias current and three priming iontophoretic pulses (50-s TMA^+ ejection every 5 to 6 min) to stabilize at 0.3 to 1.5 mM (*11*). (**B**) Sample diffusion profiles at three iontophoretic current intensities in CA1 st. pyramidale. TMA^+ potentials were converted into concentrations by the Nikolsky equation (*11*) and analyzed with an iterative program that used a simplex algorithm. The calculated values for EVF (α) and tortuosity (λ) were independent of current density, which implies that the electrode transport number was stable throughout the experiment. Electrode spacing (range, 66 to 150 μm) in agar did not influence the calculated transport number. (**C**) Comparison of TMA^+ diffusion profiles in agar and in st. pyramidale of CA1 and CA3. Dots represent measured extracellular TMA^+ concentration, whereas the solid lines show theoretical curves based on the mean parameters from three trials. The steeper rise and the larger increase for the curve obtained in CA1 indicate a smaller volume fraction in this area. The lower trace illustrates the diffusion profile of TMA^+ in agar. Each curve was computed (*11*) with the specific parameters: *D*, 1.11×10^{-5} cm^2 s^{-1}; *n*, 0.253; *I*, 130 nA; and *r*, 90 μm; the values of α and λ shown on the figure.

Our findings have two implications for hippocampal physiology. First, the combination of an already low EVF and the observed marked response to an elevation in $[K^+]_o$ can help explain the vulnerability of the CA1 region to cell damage after ischemia or hypoxia, which cause a rise in $[K^+]_o$ (*5, 16*), and the development of epileptic seizures (*7, 17, 18*). Indeed, the relative susceptibility of the three hippocampal subregions to develop interictal bursts (CA1 > dentate > CA3) in the absence of synaptic transmission (*6*) is inversely related to their EVF (Table 1). Shrinkage of extracellular space during mild hypoxia would cause (i) a rise in the interstitial concentrations of transmitters such as glutamate and glycine, and thus could lead to larger tonic activation of *N*-methyl-D-aspartate (NMDA) receptors (*19*); (ii) enhanced $[K^+]_o$ transients during cell firing, which would promote a regenerative increase in neuronal excitability (*20*); and (iii) greater synchronization of neurons by electric fields (*6, 21*) as tissue resistance rises (*7, 22*).

The second, perhaps more general, implication is that extracellular space is not a fixed fraction of total tissue volume, but varies significantly among the hippocampal subfields. In contrast, the EVF of the rat cerebellar cortex appears homogeneous (*1, 23, 24*). The basis of the observed inhomogeneity in this fundamental property of the hippocampus is not obvious, although differences in packing density among the regions examined do not seem responsible (*12*). Possible explanations would involve reduced distance between cellular membranes in CA1 st. pyramidale, additional diffusion barriers associated with the extracellular matrix in this region, or, if one assumes a fixed intercellular distance (~30 nm), an increased mean size of those objects (cell bodies, processes) that make up this region (*25*). It is not known whether regional inhomogeneity in EVF occurs elsewhere

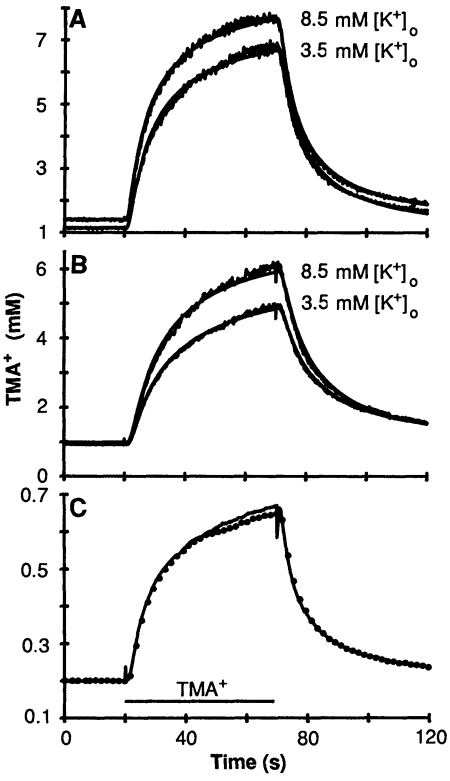

Fig. 2. Elevated extracellular K^+ reduces EVF in st. pyramidale of both CA1 and CA3. (**A**) Comparison of TMA^+ diffusion profiles in 3.5 and 8.5 mM $[K^+]_o$ demonstrates a 34% reduction in volume fraction within st. pyramidale of CA1 (from 0.121 to 0.079) with less effect on tortuosity (1.5 in 3.5 mM and 1.7 in 8.5 mM $[K^+]_o$). Diffusion parameters were I, 160 nA; r, 80 μm; n, 0.353; and D, 1.13×10^{-5} cm^2 s^{-1}. (**B**) In a different slice, EVF in st. pyramidale of CA3 was reduced by 33% (from 0.159 to 0.107) in 8.5 mM $[K^+]_o$, again without a significant change in tortuosity (1.9 in 3.5 mM, 2.0 in 8.5 mM $[K^+]_o$). The superimposed smooth curves in (A) and (B) are theoretical diffusion curves calculated from the specific parameters obtained in each experiment. Diffusion parameters were r, 80 μm; n, 0.263; D, 1.10×10^{-5} cm^2 s^{-1}; and I, 80 nA. (**C**) Elevated $[K^+]_o$ has no significant effect on TMA^+ diffusion profile or electrode transport number [n = 0.288 in 3.5 mM $[K^+]_o$ (solid line); n = 0.277 in 8.5 mM $[K^+]_o$ (dotted line)] in agar slices. Both diffusion curves (solid and dotted lines) were obtained from a single agar block where all parameters were held constant with the exception of $[K^+]_o$. I, 160 nA; r, 88 μm; and D, 1.20×10^{-5} cm^2 s^{-1}.

in the brain. A very low EVF would predispose a brain region to synchronous firing via enhancement of electric field excitation (*4, 6*). In addition, regional inhomogeneity and dynamic changes in the EVF would affect the distribution of all released chemicals over both spatial and temporal domains of the local microenvironment and could thereby modulate neural integration of synaptic signals.

REFERENCES AND NOTES

1. C. Nicholson and J. M. Phillips, *J. Physiol. (London)* **321**, 225 (1981); ———, A. R. Gardner-Medwin, *Brain Res.* **169**, 580 (1979).
2. A. Van Harreveld, in *The Structure and Function of Nervous Tissue*, G. H. Bourne, Ed. (Academic Press, New York, 1972), pp. 447–511; B. Cragg, *Neurosci. Lett.* **15**, 301 (1979); C. Nicholson and M. E. Rice, *Ann. N. Y. Acad. Sci.* **481**, 55 (1986).
3. B. R. Ransom, C. L. Yamate, B. W. Connors, *J. Neurosci.* **5**, 532 (1985); U. Heinemann and I. Deitzel, *J. Neurophysiol.* **52**, 421 (1983); I. Dietzel and U. Heinemann, *Ann. N.Y. Acad. Sci.* **481**, 72 (1986); J. D. Green, *Physiol. Rev.* **44**, 561 (1964).
4. I. Dietzel *et al.*, *Exp. Brain Res.* **40**, 432 (1980); *ibid.* **46**, 73 (1982); I. Dietzel, U. Heinemann, H. D. Lux, *Glia* **2**, 25 (1989).
5. A. J. Hansen and C. E. Olsen, *Acta Physiol. Scand.* **108**, 355 (1980).
6. R. W. Snow and F. E. Dudek, *Brain Res.* **298**, 382 (1984); C. P. Taylor and F. E. Dudek, *Science* **218**, 810 (1982); J. G. R. Jeffrys and H. L. Haas, *Nature* **300**, 448 (1982). Although the order of seizure susceptibility depends on the model, hippocampal slices bathed in low Ca^{2+}, high Mn^{2+}, or high Mg^{2+} concentrations (which removes active synapses) produce synchronized bursting in the following order: CA1 > dentate > CA2 > CA3. Synchronization in this model is presumed to result from electrical interactions among neurons, which should be influenced by the relative spacing between neuronal elements in the regions.
7. S. F. Traynelis and R. Dingledine, *J. Neurophysiol.* **59**, 259 (1988); *ibid.* **61**, 927 (1989).
8. Y. Yaari, A. Konnerth, U. Heinemann, *ibid.* **56**, 424 (1986).
9. EVF = V_o/V, where V is the total volume of tissue and V_o is the extracellular component. The tortuosity is related to the increase in path length of a diffusing particle in a complex medium compared to that in a simple one such as dilute agar. Nicholson and Phillips (*1*) called EVF α and tortuosity λ. Tortuosity reduces the diffusion coefficient of small monovalent extracellular ions by a factor of λ^2. EVF and tortuosity are independent tissue properties averaged over a distance of tens of micrometers, so they are unaffected by the microheterogeneity (for example, extracellular glycoproteins that are distributed differentially) that must exist at submicrometer distances.
10. Hippocampal slices (450 μm thick) were prepared from 1.5- to 4-month-old Sprague-Dawley rats (*7*). Slices were held in an interface chamber and perfused at a rate of 0.5 ml/min with the following medium: 130 mM NaCl, 24 mM $NaHCO_3$, 3.5 mM KCl, 1.25 mM NaH_2PO_4, 1.5 mM $CaCl_2 \cdot 2H_2O$, 1.5 mM $MgSO_4 \cdot 7H_2O$, 10 mM glucose, 0.2 mM TMA at 31° to 35°C. In some experiments $[K^+]_o$ was elevated from 3.5 to 8.5 mM by addition of 1 M KCl to the normal medium. In those experiments where $[K^+]o$ was elevated, the Schaffer collateral pathway was sectioned to prevent interictal spike invasion or seizure initiation in CA1 (*7*) and consequent ion interference.
11. Iontophoretic micropipettes (dc resistances, 5 to 15 megohms) were filled with 1 M TMA chloride. A bias current of +20 nA was continually applied to eject a small amount of probe, thus preventing dilution of TMA^+ concentration within the pipette tip, which would result in a variable transport number. Ion-selective micropipettes were made with Corning K^+ exchanger 477317 [chosen because of its high selectivity for TMA^+ over endogenous monovalent cations (*4*)] and were calibrated both before and after the experiment in standard perfusate and four concentrations of TMA^+. The electrode slope was calculated from the Nikolsky equation $E = m \log (C + C_{int})$, where E is the potential recorded, m is the electrode slope, C is the concentration of sensed ion, and C_{int} is the sum of the other ion interferences. C_{int} was 0.192 mM (n = 46) and 0.910 mM (n = 22) for 3.5 mM and 8.5 mM K^+, respectively. The electrode sensitivity (slope ± SEM) was 54.8 ± 0.6 and 59.2 ± 0.7 mV per tenfold change in TMA^+ concentration under the two $[K^+]_o$, respectively. In experiments where $[K^+]_o$ was raised, the ion-sensitive electrode was calibrated in both standard (3.5 mM) and elevated (8.5 mM) $[K^+]_o$. Before we made the measurement of diffusion profiles in brain, in each experiment the diffusion of probe in dilute (0.3%) agar was examined to determine the electrode characteristics. Diffusion profiles at three different current intensities (typically 160, 130, and 100 nA) were analyzed to determine whether the probe moved according to the diffusion equation. If α and λ are assumed to be 1.0 in agar (*1*), the diffusion coefficient D and transport number n can be calculated from the best fit of the equation $C(r,t) = (In/F)(\lambda^2/4\pi D\alpha r) \cdot \mathrm{erfc}(r\lambda/2(Dt)^{1/2})$, where $C(r,t)$ represents the TMA concentration at a given point in time (t) and distance (r) from the iontophoretic source, erfc is the complementary error function: I, n, r, and F are the iontophoretic current, transport number, electrode spacing, and Faraday's constant, respectively (*1*). The fit of the diffusion profiles to this equation was analyzed by least-squares comparison of the data to a theoretical curve. The fit was accepted only if the calculated diffusion coefficient D was within 5% of the reported value (1.14×10^{-5} cm^2 s^{-1}) (*1*). In 56 valid experiments, the average measured value of D was $1.20 \pm 0.01 \times 10^{-5}$ cm^2 s^{-1} (mean ± SEM). The transport number n was calculated from several trials at different current intensities or distances for each electrode (n = 0.332 ± 0.010 from 56 trials). The electrode array was then moved from agar slice to brain slice and similar diffusion profiles were analyzed for determination of α and λ, setting D and n at their fixed values measured in agar. The influence of irreversible washout of probe to the bathing medium was accounted for by a first-order process that acted to remove a constant proportion of probe and was incorporated into the above equation (*1*). The removal term was small enough in most cases to be neglected in the calculation of α and λ, as shown previously (*1*), although it was typically required to fit the falling phase of the TMA^+ diffusion profile. The average value of this removal term in our experiments ($1.28 \pm 0.007 \times 10^{-2}$ s^{-1} for CA1 st. pyramidale) was higher than the uptake observed for the turtle cerebellum in vivo (*1*), which is likely because of the short distance of the source electrode to an infinite sink (the medium bathing the slice). In the calculation of α and λ, each trial represents the average determined from three diffusion curves generated at three current intensities. Values of α and λ obtained were analyzed with single factor ANOVA and associated post hoc tests. Experiments involving raised K^+ were analyzed with a paired t test. Differences were considered significant at $P < 0.05$.
12. C. J. McBain, S. F. Traynelis, R. Dingledine, unpublished data.
13. Although EVF as calculated is averaged over a scale of micronmeters and thus might be influenced by cell body packing density, this effect is apparently not great, since the relative packing density (*14*) is dentate gyrus > CA1 > CA3, whereas the relative EVF is CA3 > dentate > CA1 (Table 1).
14. B. D. Boss, K. Turlejski, B. B. Stanfield, W. M. Cowan, *Brain Res.* **406**, 280 (1987); A. Mouritzen-Dam, M. Hertz, T. G. Bolwig, *ibid.* **193**, 268 (1980).
15. E. C. Zuckerman and G. H. Glaser, *Exp. Neurol.* **20**, 87 (1968).
16. M. E. Morris, *Can. J. Physiol. Pharmacol.* **52**, 872 (1974); A. J. Hansen, *Acta Physiol. Scand.* **99**, 412 (1977); K. Kawasaki, S. F. Traynelis, R. Dingledine, *J. Neurophysiol.* **63**, 385 (1990).
17. J. G. Tasker and F. E. Dudek, *Soc. Neurosci. Abstr.* **701**, 1989.
18. R. D. Andrew, M. Fagan, B. A. Ballyk, B. A. Rosen, *Brain Res.* **498**, 175 (1989); H. Baran, H. Lassmann, G. Sperk, F. Seitelberger, O. Hornykiewicz, *Neuroscience* **21**, 679 (1987).
19. P. Sah *et al.*, *Science* **246**, 815 (1989).
20. Hyperosmotic agents restricted to the extracellular space suppress electrographic seizures caused by 8.5 mM $[K^+]_o$, presumably by expanding the extracellular space, since membrane-permeant analogs were ineffective (*7*). Analyses of diffusion curves after addition of medium-made hyperosmotic with 30 mosM mannitol in the continued presence of 8.5 mM $[K^+]_o$ shows that a small expansion (~10%) occurred in the extracellular space of CA1 st. pyramidale (control: α, 0.095 ± 0.034, n = 9; in mannitol: α, 0.105 ± 0.037, n = 9). The percent expansion of EVF is of similar magnitude to the fall in tissue resistance (8.9%) produced by 30 mosM mannitol (*7*).

21. J. G. R. Jeffrys, *J. Physiol. (London)* **319**, 143 (1981).
22. J. Holsheimer, *Exp. Brain Res.* **67**, 402 (1987).
23. Subfield inhomogeneity occurs in the frog retina, where calculations of α derived from resistivity measurements suggest that EVF in this area can be as low as 0.028 (*24*). These calculations, however, assumed a value for tortuosity based on previous measurements in rat cerebellum (*1*) and assumed that tortuosity was identical in all retinal regions.
24. C. J. Karwoski, D. A. Frambach, L. M. Proenza, *J. Neurophysiol.* **54**, 1607 (1985).
25. The EVF can be shown algebraically to be a function of the mean size of objects (cells and processes) occupying the space and the mean distance between objects. If the objects occupying extracellular space are modeled as cubes of width w, EVF = $\Sigma A_n[(w_n + d)^3 - w_n^3]/(w_n + d)^3$, where n is the number of different-sized objects, A_n is the fraction of each object ($\Sigma A_n = 1$), and d is the mean interobject distance. Given fixed d = 30 nm, if the space were occupied only by cubes of width 450 nm (for example, processes), EVF = 0.176; however, with cubes of 10-μm width (cell bodies), EVF = 0.009. With an equal number of large and small cubes, EVF = 0.102. The essential point is that the smaller the mean size of objects, the larger the expected EVF. Further tests of this analysis would require quantitative measurements from electron micrographs of the different hippocampal regions.
25. Supported by NIH grant NS17771 and the Klingenstein Fund. We thank J. O. McNamara and P. A. Schwartzkroin for helpful comments and C. Nicholson for kindly providing the simplex algorithm.

20 February 1990; accepted 18 May 1990

Expression of T Cell Antigen Receptor Heterodimers in a Lipid-Linked Form

AUGUSTINE Y. LIN,* BRIGITTE DEVAUX, ADRIENNE GREEN, CHARLES SAGERSTRÖM, JOHN F. ELLIOTT,† MARK M. DAVIS

The interaction of the T cell receptor for antigen (TCR) with its antigen–major histocompatibility complex ligand is difficult to study because both are cell surface multimers. The TCR consists of two chains (α and β) that are complexed to the five or more nonpolymorphic CD3 polypeptides. A soluble form of the TCR was engineered by replacing the carboxyl termini of α and β with signal sequences from lipid-linked proteins, making them susceptible to enzymatic cleavage. In this manner, TCR heterodimers can be expressed independently of the CD3 polypeptides and in significant quantities (0.5 milligram per week). This technique seems generalizable to biochemical and structural studies of many other cell surface molecules as well.

THE ANTIGEN-SPECIFIC IMMUNE RESPONSES of vertebrates are determined by B and T lymphocytes. B cell specificity is due to immunoglobulin molecules that can be either expressed on the cell surface or secreted. Extensive information has been obtained regarding the biochemistry and structure of immunoglobulins and their interactions with various antigens (*1, 2*). In contrast, little is known about the structure of TCR heterodimers or their interaction with their putative ligands, antigen fragments embedded in molecules of the major histocompatibility complex (MHC) (*3*). This is in part because the TCR is not secreted, and it is not expressed on the surface of T cells in large amounts [~20,000 to 40,000 molecules per cell (*4*)]. The complexity of the TCR ligand and its normal cell surface expression has also contributed to the difficulties in trying to characterize the mode of interaction. In addition, although the TCR polypeptides are immunoglobulin-like (*5*), they are always co-expressed with CD3 molecules (*6*), which leaves open the possibility that they require those molecules for their stability. To better understand TCR-mediated recognition, we and others have unsuccessfully tried to engineer TCR α and β polypeptides, or variable (V) regions derived from them, as antibody chimeras (7) or truncated molecules (*8*), to allow the expression of a soluble form in biochemically significant quantities.

The COOH-terminal 37 amino acids of decay-accelerating factor (DAF) can serve as a signal sequence for the attachment of an otherwise secreted protein to the cell surface by means of a phosphotidyl inositol (PI)–glycan linkage (*9*), which can be cleaved off the surface of transfected cells by the specific enzyme, phosphatidyl inositol–specific phospholipase C (PI-PLC) (*10*). Expression of a recombinant TCR heterodimer anchored by a PI-glycan linkage would provide: (i) a PI-PLC–cleavable, soluble form without a need for detergents; (ii) TCR surface expression that is not limited by the amount of CD3 (*11*); and (iii) a lipid-linkage that should keep the TCR polypeptides in the correct orientation with respect to each other and at a relatively high concentration (in the plane of the interior membrane), thus maximizing the chances of correct association.

The T helper hybridoma 2B4 (*12, 13*) bears an αβ TCR that recognizes a fragment of pigeon cytochrome c plus the class II MHC molecule, I-E^k (*14*). We replaced the transmembrane and cytoplasmic domains of both chains with either the signal sequence from a monomeric protein, DAF (*8*), or with COOH-termini derived from human placental alkaline phosphatase (HPAP) (*15*), a PI-linked dimer. Because the sequences required for HPAP to direct PI-linkage have not been defined, we designed two HPAP signals of different lengths that contained either the last 38 (HPAP-S) or the last 47 amino acids (HPAP-L) of the protein (Fig. 1A). By analogy with immunoglobulin Fab fragments, all three PI-anchoring signal sequences were joined to the TCR chains at the fifth residue COOH-terminal of the last conserved cysteine. The modified α and β cDNAs were then inserted into the mammalian expression vector pBJ1-Neo (*16*). Staining of COS cell transfectants with monoclonal antibodies specific for the α [A2B4.2, (*13*)] and the β [KJ25, anti-$V_\beta 3$ (*17*)] TCR chains revealed the presence of both on the cell surface. Ninety percent of the TCR molecules could be cleaved from the membrane after treatment of the cells with PI-PLC from *Bacillus thuringiensis* (*10*), thus all the COOH-termini used here could serve as signal sequences for this type of linkage. The same constructs were then introduced into Chinese hamster ovary (CHO) cells, and stable transfectants resistant to the antibiotic, G418, were selected.

In order to determine the stability of expression of the PI-anchored TCR on the cell surface, the brightest 5% αβ-staining cells of each pool of CHO transfectants (αβDAF, αβHPAP-S, and αβHPAP-L) were pooled after fluorescence-activated cell sorting. The same procedure was repeated on the sorted cells after 2 weeks of culture. The staining profiles obtained (Fig. 1B) after the second sorting of each CHO transfectant pool were obtained with subsaturating amounts of the antibody to V_α, A2B4.2, so that it would not block the binding of the antibody to $V_\beta 3$, KJ25 [(*18*) and below]. At this point, αβHPAP-S cells were a homogeneous population of bright double-positive cells, whereas both the αβDAF and αβHPAP-L cells contained significant numbers of dully staining cells (Fig. 1B). This suggests that the HPAP sequences, especial-

A. Y. Lin, B. Devaux, A. Green, M. M. Davis, Howard Hughes Medical Institute and the Department of Microbiology and Immunology, Stanford University School of Medicine, Stanford, CA 94305–5402.
C. Sagerström and J. F. Elliott, Department of Microbiology and Immunology, Stanford University School of Medicine, Stanford, CA 94305–5402.

*Present address: T Cell Sciences, Cambridge, MA 02138.
†Present address: Department of Medical Microbiology and Infectious Diseases, University of Alberta, Edmonton, Canada T6G 2H7.